Optical properties of normal and cancerous human skin in the visible and near-infrared spectral range

Elena Salomatina
Massachusetts General Hospital
Wellman Center for Photomedicine
70 Blossom Street
Boston, Massachusetts 02114

Brian Jiang
Harvard Medical School
Beth Israel Deaconess Medical Center
Shapiro Clinical Center
330 Brookline Avenue
Boston, Massachusetts 02134

John Novak
Wellman Center for Photomedicine
Harvard Medical School
70 Blossom Street
Boston, Massachusetts 02114

Anna N. Yaroslavsky
Harvard Medical School
Massachusetts General Hospital
Wellman Center for Photomedicine
55 Fruit Street
Boston, Massachusetts 02114

Abstract. Differences in absorption and/or scattering of cancerous and normal skin have the potential to provide a basis for noninvasive cancer detection. In this study, we have determined and compared the *in vitro* optical properties of human epidermis, dermis, and subcutaneous fat with those of nonmelanoma skin cancers in the spectral range from 370 to 1600 nm. Fresh specimens of normal and cancerous human skin were obtained from surgeries. The samples were rinsed in saline solution and sectioned. Diffuse reflectance and total transmittance were measured using an integrating sphere spectrophotometer. Absorption and reduced scattering coefficients were calculated from the measured quantities using an inverse Monte Carlo technique. The differences between optical properties of each normal tissue-cancer pair were statistically analyzed. The results indicate that there are significant differences in the scattering of cancerous and healthy tissues in the spectral range from 1050 to 1400 nm. In this spectral region, the scattering of cancerous lesions is consistently lower than that of normal tissues, whereas absorption does not differ significantly, with the exception of nodular basal cell carcinomas (BCC). Nodular BCCs exhibit significantly lower absorption as compared to normal skin. Therefore, the spectral range between 1050 and 1400 nm appears to be optimal for nonmelanoma skin cancer detection.
[DOI: 10.1117/1.2398928]

Keywords: skin; cancer; scattering; absorption; integrating sphere spectrophotometry; inverse Monte Carlo technique.

Paper 06035R received Feb. 23, 2006; revised manuscript received Jun. 22, 2006; accepted for publication Aug. 23, 2006; published online Nov. 20, 2006.

1 Introduction

Nonmelanoma skin cancers, including basal cell carcinomas (BCCs) and squamous cell carcinomas (SCCs), are more common than all other types of human cancers. These cancers have an intrinsically low optical contrast in the visible spectral range. A number of techniques[1–7] and contrast agents[8–10] have been suggested and tested for the detection and delineation of these tumors. So far the best results were yielded with methods that employ exogenous contrast agents.[11,12] However, if a method capable of resolving subtle differences in the optical properties of endogenous chromophores of normal and cancerous tissues was available, this would be a great asset for tumor detection. Thus far, to the best of our knowledge, the optical properties of nonmelanoma skin cancers have not been reported so far. The optical properties of normal skin have been investigated by several groups.[13–15] However, most of the investigators studied either the optical properties of dermis and subcutaneous fat,[16] or reported on the combined optical properties of epidermis and dermis.[17,18] Data on the optical properties of epidermis are rare.[19]

In this study, we have determined and compared the optical properties of normal skin layers to those of nonmelanoma skin cancers in the wide spectral range from 370 to 1600 nm with the purpose of selecting the spectral range where the differences between cancer and normal tissue are maximal. We employed integrating sphere spectrophotometry combined with the inverse Monte Carlo technique. At least five samples of each tissue type, including epidermis, dermis, subcutaneous fat, nodular BCC, infiltrative BCC, and invasive SCC, were measured. The resulting optical properties of different tissue types were compared. The differences in scattering and absorption between each normal and cancerous tissue type were statistically analyzed using an unpaired two-tailed *t*-test, and the spectral ranges where these differences were maximal identified.

2 Materials and Methods

2.1 *Sample Preparation*

Freshly discarded specimens of normal and cancerous human skin were obtained from the surgeries under an institutional review board–approved protocol. The time between the surgical removal of the skin and the measurements did not exceed

Address correspondence to Anna N. Yaroslavsky, Harvard Medical School, Wellman Center for Photomedicine, Massachusetts General Hospital, 55 Fruit St., BAR314B, Boston, MA 02114; Tel: 617-726-1590; Fax: 617-724-2075; E-mail: Yaroslav@helix.mgh.harvard.edu

1083-3668/2006/11(6)/064026/9/$22.00 © 2006 SPIE

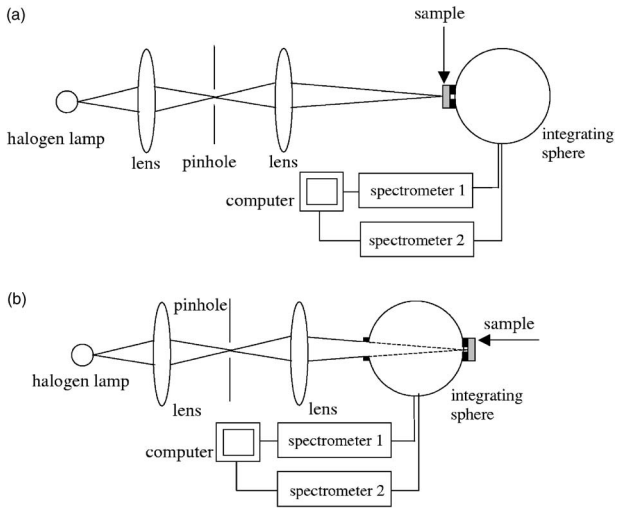

Fig. 1 Experimental arrangement for total transmittance (a) and diffuse reflectance (b) measurements.

7 h. Skin excisions from the face, scalp, neck, and back of the patients were used for the experiments. The samples were briefly rinsed in Dulbecco's phosphate-buffered saline (pH 7.4) solution and sectioned using a microcryotome. Sections were cut parallel to the tissue surface. We measured the thickness of each section using a high-precision digital micrometer (Mitutoyo Corp., Kawasaki, Japan) with the accuracy of ± 1 μm. The thickness of the epidermis, dermis, fat, and cancerous tissues sections varied between 60 and 100 μm, 100 and 780 μm, 280 and 800 μm, and 170 and 850 μm, respectively. The lateral size of the sectioned tissues was in the 6- to 17-mm range. Sectioned specimens were hydrated with saline and sealed between a microscopic slide and a coverslip with rapid mounting media for microscopy Entellan New (Electron Microscopy Science, Hatfield, Pennsylvania) to prevent desiccation. In total, 7 epidermis, 8 dermis, 10 subcutaneous fat, 6 infiltrative BCC, 5 nodular BCC, and 8 SCC specimens were investigated.

2.2 *Integrating Sphere Spectrophotometry*

The integrating sphere spectrophotometric system was constructed for the diffuse reflectance and total transmittance measurements of skin specimens. The experimental arrangements are presented in Figs. 1(a) and 1(b). We have chosen a single-integrating sphere configuration to avoid light interactions between the spheres.[20] For measuring total transmittance and diffuse reflectance, the light from a halogen lamp (HL-2000-HP-FHSA, Ocean Optics, Dunedin, Florida) was focused onto the sample, which was mounted on the entrance and exit ports of the integrating sphere (4P-GPS-033-SL, Labsphere, North Sutton, New Hampshire), respectively. The lateral size of the investigated sample always exceeded the diameter of the respective sphere port. The diameter of the beam on the sample did not exceed 3 mm. For the samples with lateral sizes between 6 and 7 mm, the size of the beam was reduced to 2 mm. The light diffusely reflected and transmitted by the sample was detected by two charge-coupled device–based spectrometers connected via the optical fibers to the detector ports. We have used a HR2000 spectrometer (Ocean Optics) in the 370- to 980-nm region and an EPP2000-NIR InGaAs spectrometer (StellarNet, Tampa, Florida) in the 900- to 1600-nm spectral range. The wavelength calibration of the spectrometers was performed using a Hg(Ar) calibration lamp (HG-1 Mercury Argon Calibration Source, Ocean Optics) with an accuracy better than 1 nm. For all the measurements, a signal-to-noise ratio was not worse than 200:1. To ensure that the same area of the sample was examined, all the slides were marked with a permanent marker around the investigated area during the first measurement.

2.3 *Confocal Imaging*

To verify that the skin specimens contained only one type of tissue (i.e., epidermis, dermis, fat, or cancer), each section was imaged using reflectance confocal microscopy. The exact same area of the sample that corresponded to the region measured during the integrating sphere experiments was examined. The confocal microscope that was used for verification experiments was described in detail elsewhere.[5] Confocal images were acquired at the wavelength of 656 nm. Water immersion $20\times/0.75$ objective (Nikon, Japan) was employed. The system provided an axial resolution of 5 μm, and lateral resolution of 1.2 μm. Confocal images were acquired from both the front and the back sides of the samples at a depth of 10 μm. Single confocal images covered the area of 800×600 μm^2. To identify the tissue type, confocal mosaics were created from sequences of single images of adjacent areas. These mosaics covered an area of 8×6 mm^2. Reflectance confocal microscopy provided high-quality images of the sections. Distinctive features of skin layers can be clearly seen in these images. The samples that contained more than one tissue type were discarded.

2.4 *Data Processing Technique*

We have used an inverse Monte Carlo technique to recover the optical properties of the samples from the measured quantities of diffuse reflectance and total transmittance.[21] The technique employs a combination of a quasi-Newton inverse algorithm[22] and a forward Monte Carlo simulation.[21,23] The inverse quasi-Newton algorithm is an iterative optimization technique that combines rapid local convergence of the Newton method with the ability to achieve proximity of the solution if the initial approximation is poor. In most practical cases, the algorithm required less than 10 iterations to converge. The forward Monte Carlo method is based on the numerical simulation of photon transport in scattering media. The algorithm takes into account exact optical and geometrical configuration of experiment: mismatch of the refractive indices on the boundaries of the sample, light losses at the edges of the sample, finite beam diameter and port dimensions of the integrating sphere, and arbitrary angular distribution of the incident light. Interpretation of all the experimental data obtained in this study was conducted under the assumption of the Henyey-Greenstein scattering phase function. The anisotropy factor g was assumed to be 0.8 and the refractive index to be 1.4 for all the skin layers in the entire spectral range investigated.[24–26,14]

2.5 *Statistical Analysis*

A Student's unpaired two-tailed *t*-test (STATISTICA 6.0, StatSoft, Inc, Tulsa, Oklahoma) was used to evaluate the significance of the difference between obtained optical properties of healthy skin layers and cancerous tissues. The differences between optical coefficients of normal and cancerous tissues were considered to be statistically significant when the calculated probability value (p value) was equal or less than 0.05. P value $\leqslant 0.05$ means that the probability that the two data sets are different is $\geqslant 95\%$. This level of significance is considered acceptable for the biological samples. Calculated p values were plotted against the wavelength to identify the spectral regions, where the optical properties of normal and cancerous tissues differed significantly.

3 Results and Discussion

In total, we have measured and analyzed 7 samples of human epidermis, 8 samples of dermis, 10 samples of subcutaneous fat, 5 samples of nodular BCC, 6 samples of infiltrative BCC, and 8 samples of invasive SCC. All the samples were measured in the spectral range from 370 to 1600 nm. Averaged absorption and reduced scattering coefficients for each of the examined tissue types were calculated using the inverse Monte Carlo technique. The results are presented in Figures 2–11.

Absorption and scattering coefficients of healthy skin layers are shown in Figs. 2(a), 3(a), and 4(a). The graphs demonstrate that the scattering of normal skin layers decreases with the increasing wavelength. The steady decrease can be explained by the decrease of the contribution of Rayleigh scattering, whereas the contribution of Mie scattering increases with the increasing wavelength.[27] For all the tissues investigated, we have noticed an increase of scattering coefficient in the vicinity of the strong water absorption band around 1450 nm. Similar behavior of the absorption and scattering coefficients can be seen in the graphs presented in Refs. 28 and 29 for human blood, gallbladder, and bile. As experimental conditions and/or models of light propagation used to derive the optical properties in the referenced literature and our work were different, it is more likely that the obtained results manifest the general optical property of the tissues, rather than the evidence of some cross talk between the two parameters in the measurements and calculations. This correlation in the behavior of absorption and scattering may be caused by the existing relation between the real and imaginary parts of the dielectric constant. However, more detailed investigation of the observed phenomenon is required to confirm or refute our hypothesis.

The scattering of epidermis is noticeably higher than the scattering of dermis and subcutaneous fat in the entire wavelength range. It is known that optical properties of epidermis in the range of 370 to 1200 nm are determined by melanin content.[13] For this study, we used excisions taken from Caucasian subjects with fair skin. The content of melanin in the epidermis of these skin samples was comparatively low. However, the relative refractive index of melanin with respect to the surrounding medium is approximately 1.3.[30] Therefore, light scattering in the epidermis is significantly higher than in other skin tissues. In the dermis, scattering is predominantly caused by collagen fibers and their associated small structures.[31] The irregular bundles of thick collagen and elastin fibers can be clearly seen in the confocal image of the dermis [Fig. 3(b), the gray arrow points toward the fibers]. The scattering properties of subcutaneous fat are also affected by the presence of connective tissue septa composed of collagen and elastin. In the confocal image of subcutaneous fat [Fig. 4(b)], the septum separating conglomerates of fat cells—adipocytes—is shown with black arrows. It was noticed that the scattering properties of fat differed depending on the body area from which the excisions were taken. The collagen-elastin net appeared thicker and denser in the subcutaneous fat samples obtained from the facial or scalp area [Fig. 5(a), collagen bundles are shown with black arrows]. The presence of collagen and elastin resulted in increased scattering coefficients [Fig. 5(c)]. Skin excisions taken from the back of the subjects revealed fat with large multilocular adipocytes and very thin connective tissue septa [Fig. 5(b)]. In this case, scattering was much lower [Fig. 5(c)].

Absorption spectra of normal skin layers are presented in Figs. 2(a), 3(a), and 4(a). In the visible wavelength range, melanin determines absorption in the epidermis. Absorption of melanin is monotonously decreasing with the increase of the wavelength. Therefore, the effect of melanin on epidermis absorption properties is more pronounced at shorter wavelengths. Hemoglobin dominates absorption properties of dermis and fat in the visible spectral range. Hemoglobin absorption peaks around 410 and 540 nm appear consistently in the spectra of dermis and fat, as all the specimens, except the epidermal, contained some blood. Absorption of the epidermis, dermis, and fat in the near-infrared region is determined by water and lipid content. In the proximity of 1200 nm, water and lipid absorption bands overlap. Therefore, this peak is more pronounced for the subcutaneous fat as compared to the epidermis and dermis. At the same time, the epidermis and dermis exhibit stronger absorption in the range from 1350 to 1600 nm.

In Figs. 6(a), 7(a), and 8(a), absorption and scattering properties of cancerous tissues are presented. Scattering of all investigated nonmelanoma skin tumor types demonstrate qualitatively similar behavior. It gradually decreases with the increasing wavelength. Quantitatively, infiltrative BCC is characterized by a higher scattering coefficient in comparison with the scattering of nodular BCCs and SCCs. The higher scattering coefficient of infiltrative BCC may be explained by its structural characteristics. Typically, these tumors have thin strands or cords of tumor cells extending into the surrounding highly scattering dermis. The scattering of squamous cell carcinomas is consistently lower than the scattering of both types of BCCs in the entire wavelength range.

Absorptive properties of nonmelanoma skin cancers are determined by melanin and hemoglobin in the visible spectral range and by water in the near-infrared spectral range. Depositions of melanin often occur in the nonmelanoma tumors.[10] The presence of this chromophore strongly affects absorption and scattering of the tumors. However, in general, the content of both melanin and hemoglobin in nonmelanoma skin cancers is highly variable. Therefore, the contrast based on the differences in melanin and hemoglobin content of the tumors as compared to normal skin tissues cannot be expected to occur reproducibly. We have found that on average, nodular BCCs contain less blood as compared to infiltrative BCCs and

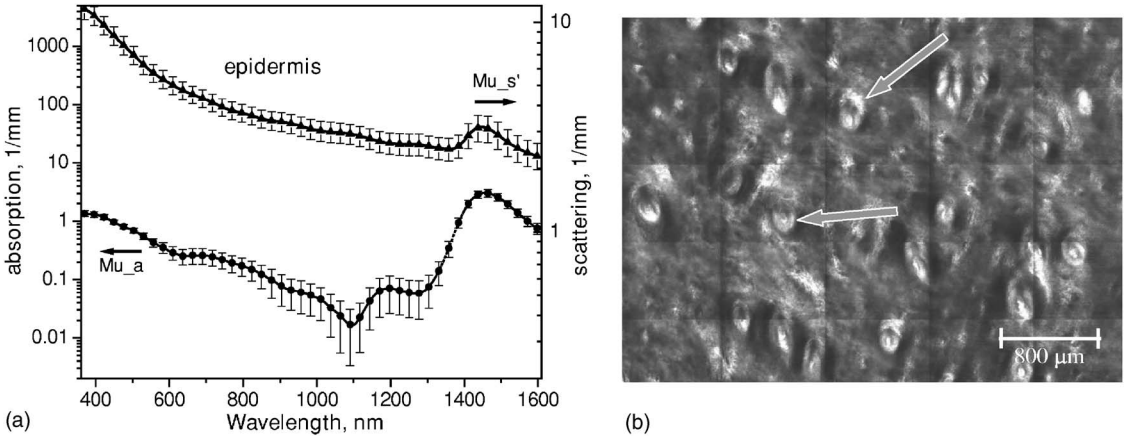

Fig. 2 (a) Optical properties of epidermis. Triangles—reduced scattering coefficients, circles—absorption coefficients, bars—standard errors. Averaged over seven samples. (b) Typical confocal image of epidermis; arrows point to hair follicles.

SCCs. We also noted that infiltrative BCCs are characterized by a slightly higher absorption than SCCs in the range from 600 to 1600 nm. Absorption of nodular BCCs is lower than that of infiltrative BCCs and SCCs.

We used statistical analysis to evaluate the significance of the differences between optical properties of normal skin layers and cancerous tissues. The analysis was performed using unpaired two-tailed *t*-tests. In the resulting *p* plots, the dependences of *p* values on the wavelength are presented. The spectral regions where the differences between cancerous tissues and healthy skin layers were statistically significant ($p < 0.05$) can be clearly identified. *P* plots presented in the Figs. 9–11 show the differences between absorption and scattering properties of the healthy epidermis, dermis, fat, and nonmelanoma skin tumors, respectively. The spectral regions where optical properties of healthy and cancerous tissues differ significantly are listed in the Table 1.

In Fig. 9, the *p* plots comparing absorption [Fig. 9(a)] and scattering [Fig. 9(b)] of epidermis to those of cancerous tissues are presented. As can be seen in Fig. 9(a), the differences in absorption between the epidermis and all the types of cancer investigated are significant below 500 nm, in the vicinity of the hemoglobin Soret absorption band. As the blood content in cancerous samples is highly variable and may be affected by sample preparation technique, the identified significant differences in absorption are not likely to provide a reliable basis for tissue discrimination. At the same time, the differences in scattering between the epidermal and cancerous tissues were found to be significant in the complete spectral range investigated.

P plots in Figs. 10(a) and 10(b) show the differences in the absorption and scattering properties of the dermis and cancerous tissues, respectively. No significant differences were found in the absorption properties of the dermis and infiltrative BCC. This type of cancer is difficult to detect because, as was mentioned earlier, it is characterized by thin cancer cell strands invading the dermis. Therefore, the optical properties of infiltrative BCC are similar to those of the dermis. The differences in absorption of nodular BCCs and SCCs versus the dermis are significant in the wavelength range from 750 to 1380 nm and from 720 to 910 nm, respectively. Absorption in these cancer types was generally lower than in the

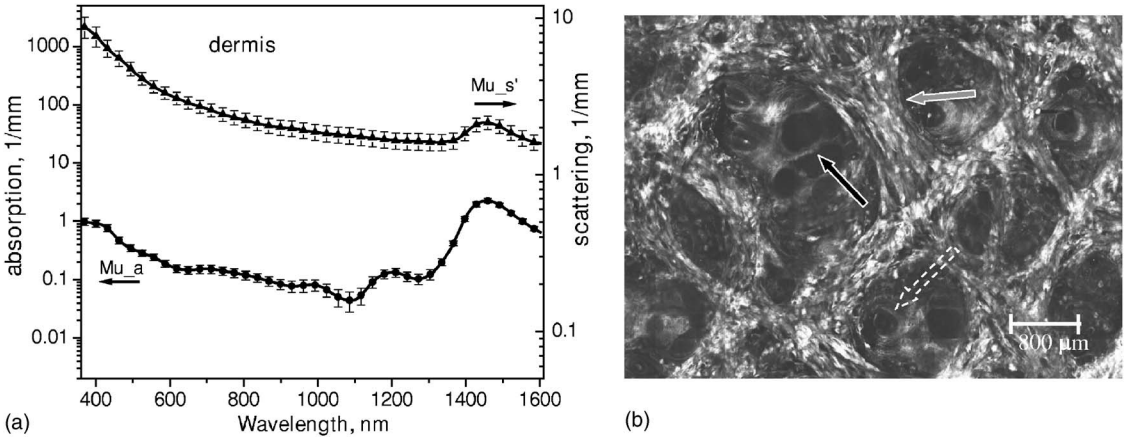

Fig. 3 (a) Optical properties of dermis. Triangles—reduced scattering coefficients, circles—absorption coefficients, bars—standard errors. Averaged over eight samples. (b) Typical confocal image of dermis; gray arrow points to collagen-elastin bundle, black arrow points to sebaceous gland, dashed arrow points to hair shaft.

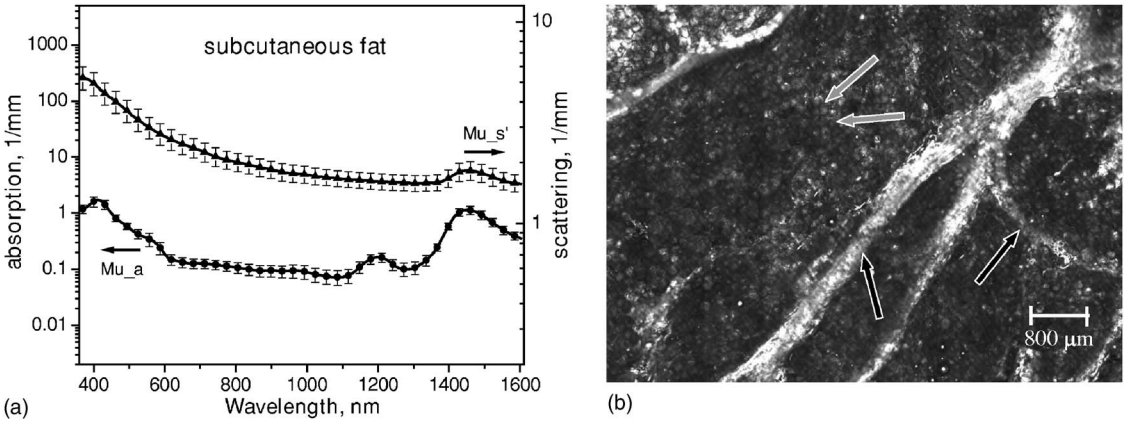

Fig. 4 (a) Optical properties of subcutaneous fat. Triangles—reduced scattering coefficients, circles—absorption coefficients, bars—standard errors. Averaged over 10 samples. (b) Typical confocal image of subcutaneous fat; gray arrows point to fat cells adipocytes, black arrow points to connective tissue septum.

dermis. *P* plots comparing scattering properties of dermis-tumor pairs reveal that the scattering properties of dermis–nodular BCC and dermis-SCC exhibit significant differences in the complete wavelength range investigated. For infiltrative BCCs, the spectral range of significant differences was much narrower and covered the wavelengths between 1050 and 1400 nm.

P plots comparing absorption properties of subcutaneous fat and cancerous specimens [see Fig. 11(a)] demonstrate that for all tumor types there exist significant differences in the regions from 370 to 500 nm and from 1400 to 1500 nm. These two regions correspond to the absorption bands of blood and water, respectively. Our results indicate that on average, cancerous tissue contains less blood and more water as compared to subcutaneous fat. Differences in scattering properties of subcutaneous fat-tumors pairs are significant for all cancer types in the wavelength range between 1050 and 1400 nm [see Fig. 11(b)].

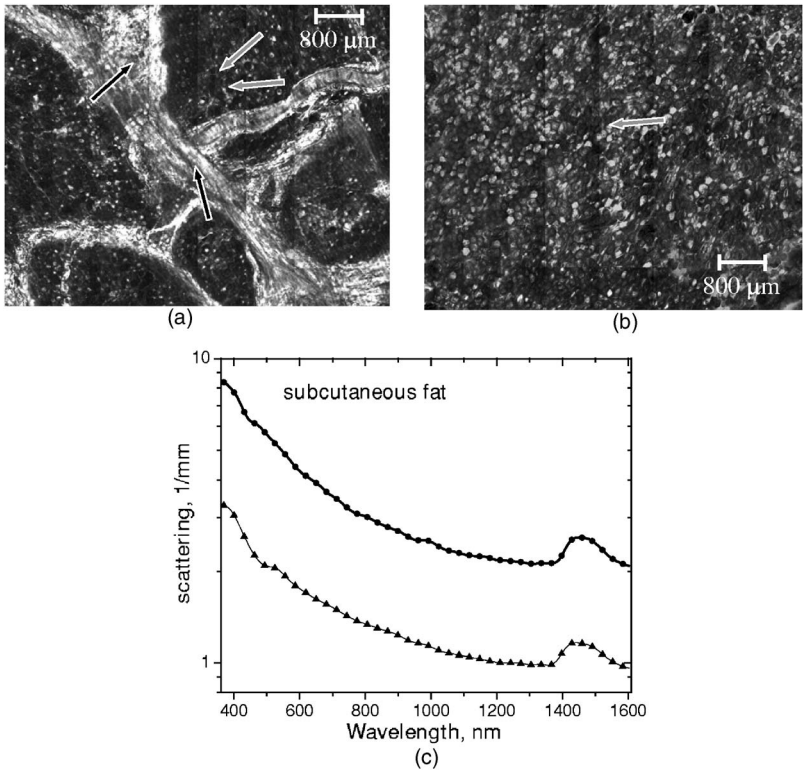

Fig. 5 (a) Confocal image of subcutaneous fat sample with dense connective tissue septa separating multilocular adipocytes (the excision was taken from the facial area); (b) confocal image of subcutaneous fat sample without the septa (the excision was taken from the back). Gray arrows point to fat cells adipocytes, black arrows point to connective tissue septum. (c) Scattering properties of subcutaneous fat. Circles—reduced scattering coefficient of fat with dense connective tissue septa, triangles—reduced scattering coefficient of fat without the septa.

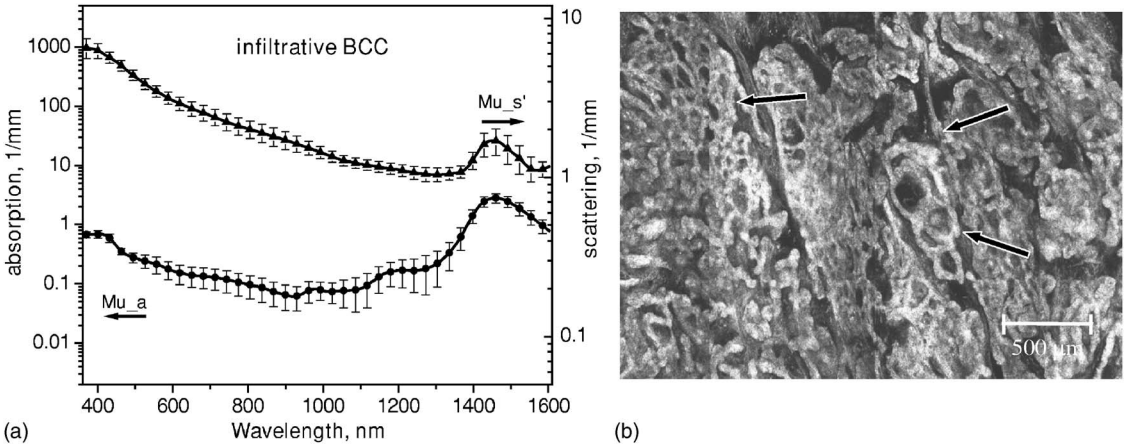

Fig. 6 (a) Optical properties of infiltrative BCC. Triangles—reduced scattering coefficients, circles—absorption coefficients, bars—standard errors. Averaged over six samples. (b) Confocal image of infiltrative BCC specimen; arrows point to the strands of tumor cells.

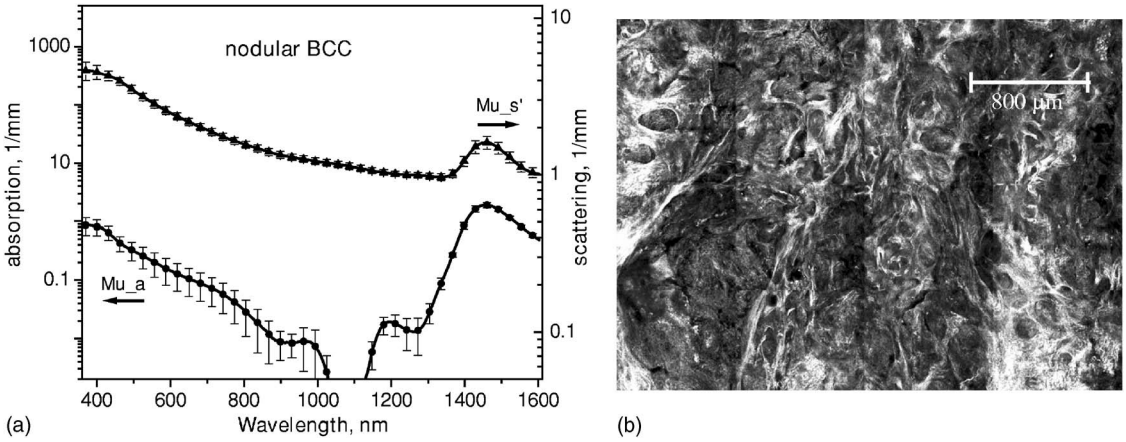

Fig. 7 (a) Optical properties of nodular BCC. Triangles—reduced scattering coefficients, circles—absorption coefficients, bars—standard errors. Averaged over five samples. (b) Confocal image of nodular BCC specimen.

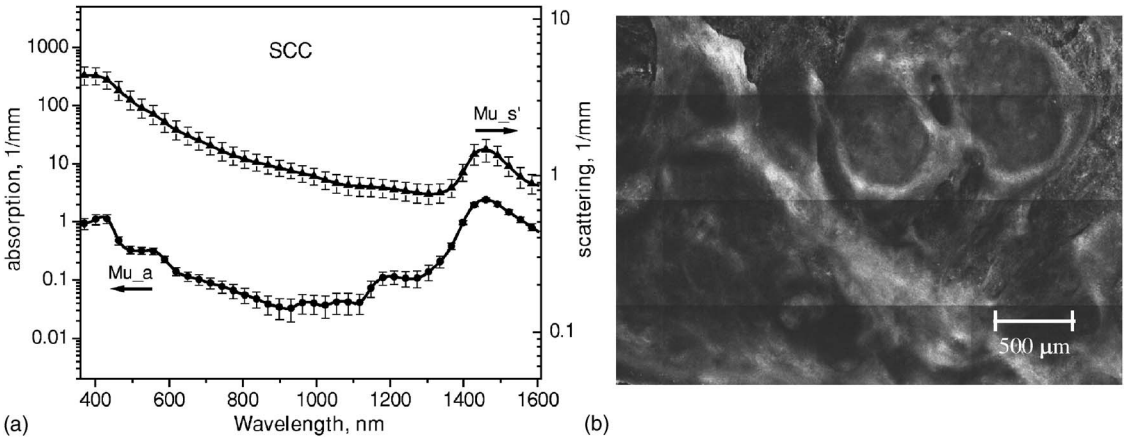

Fig. 8 (a) Optical properties of SCC. Triangles—reduced scattering coefficients, circles—absorption coefficients, bars—standard errors. Averaged over eight samples. (b) Confocal image of SCC specimen.

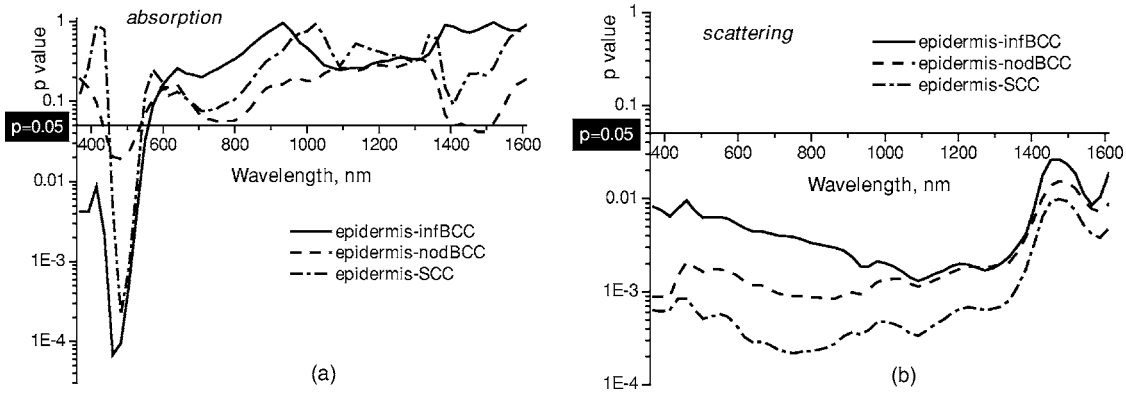

Fig. 9 *T*-test results comparing epidermis and cancerous skin absorption (a) and scattering (b) properties. Solid line—comparison of epidermis and infiltrative BCC, dashed line—comparison of epidermis and nodular BCC, dashed dotted line—comparison of epidermis and SCC absorption and scattering properties.

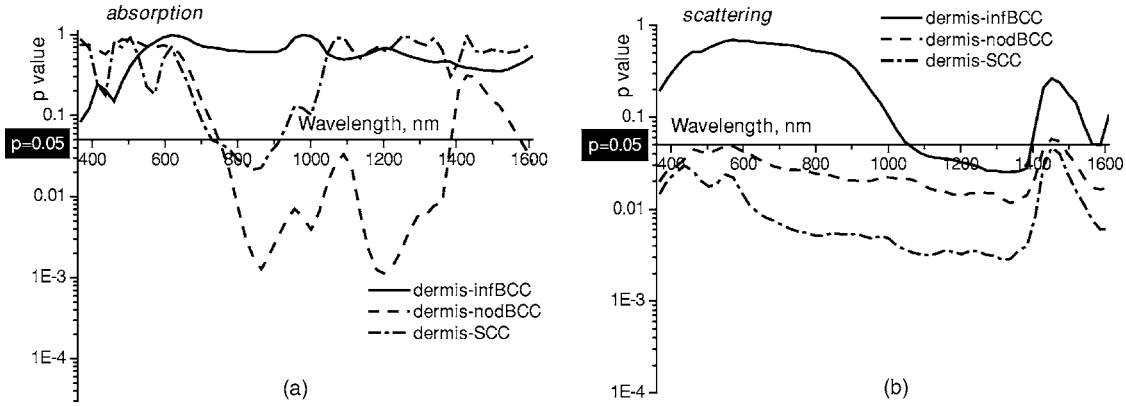

Fig. 10 *T*-test results comparing dermis and cancerous skin absorption (a) and scattering (b) properties. Solid line—comparison of dermis and infiltrative BCC, dashed line—comparison of dermis and nodular BCC, dashed dotted line—comparison of dermis and SCC absorption and scattering properties.

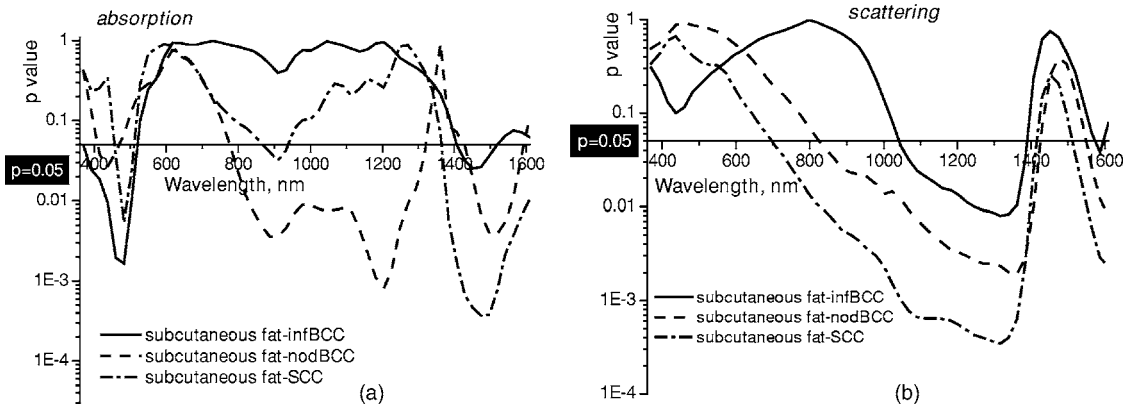

Fig. 11 *T*-test results comparing subcutaneous fat and cancerous skin absorption (a) and scattering (b) properties. Solid line—comparison of fat and infiltrative BCC, dashed line—comparison of fat and nodular BCC, dashed dotted line—comparison of fat and SCC absorption and scattering properties.

Table 1 Spectral regions of maximal optical contrast between normal and cancerous tissues.

		Epidermis	Dermis	Subcutaneous Fat
Infiltrative BCC	absorption	370 to 570 nm	no	370 to 520 nm, 1410 to 1515 nm
	scattering	370 to 1600 nm	1055 to 1400 nm	1040 to 1390 nm
Nodular BCC	absorption	430 to 540 nm, 1450 to 1520 nm	750 to 1380 nm, 1580 to 1600 nm	410 to 470 nm, 780 to 1320 nm, 1430 to 1590 nm
	scattering	370 to 1600 nm	370 to 1435 nm, 1480 to 1600 nm	820 to 1430 nm, 1525 to 1600 nm
SCC	absorption	450 to 540 nm	720 to 915 nm	450 to 510 nm, 1360 to 1600 nm
	scattering	370 to 1600 nm	370 to 1600 nm	700 to 1410 nm, 1510 to 1600 nm

The detected differences in the absorption properties of healthy skin-tumor pairs were provided by variations in the concentration of hemoglobin, melanin, and water. It has been reported previously[1,32] that variations in water absorption can be used as a reliable parameter for distinguishing nonmelanoma skin cancers. We also found significant differences in water content in all subcutaneous fat-tumor pairs. Water absorption in fat was consistently lower than that of cancerous specimens. However, other skin layers (i.e., epidermis and dermis) did not differ from cancer in terms of water content.

Statistical and comparative analysis of the differences in the optical properties of cancerous and normal skin revealed that all healthy skin layer–tumor pairs exhibited significant differences in scattering in the spectral range between 1050 and 1400 nm. Scattering in cancer specimens was substantially lower as compared to normal skin. At the same time, absorption properties of healthy and cancerous skin, with the exception of nodular BCC, which exhibited significantly lower absorption than that of normal skin, did not differ substantially in this wavelength region. Our results indicate that in the wavelength range between 370 and 1600 nm, there is no spectral region where the differences in absorption are significant for all healthy tissue–cancer pairs.

4 Conclusions

We have determined and compared absorption and scattering properties of healthy human skin layers and nonmelanoma skin cancers in the wavelength range from 370 to 1600 nm. We identified several wavelength regions where the difference in absorption and scattering properties of each healthy tissue–cancer pair were statistically significant ($p < 0.05$). The results of our study indicate that there exists no spectral region within the wavelength range investigated where the differences in absorption are significant for all healthy tissue–tumor pairs simultaneously. However, all healthy tissue–cancer pairs exhibited statistically significant differences in scattering in the wavelength range from 1050 to 1400 nm. Absorption properties of normal skin layers and cancerous specimens did not differ significantly in this region with the exception of nodular BCC–normal tissue pair. Nodular BCCs exhibit lower absorption as compared to normal skin. Thus the spectral range from 1050 to 1400 nm, where scattering properties of normal and cancerous tissues exhibit maximal difference, may provide a reliable base for pathology discrimination.

References

1. R. Woodward, V. Wallace, R. Pye, B. E. Cole, D. D. Arnone, E. H. Linfield, and M. Pepper, "Terahertz pulse imaging of ex vivo basal cell carcinoma," *J. Invest. Dermatol.* **120**, 72–78 (2003).
2. N. Lassay, A. Spatz, M. F. Avril, A. Tardivon, A. Margulis, G. Mamelle, D. Vanel, and J. Leclere, "Value of high-frequency US for preoperative assessment of skin tumors," *Radiographics* **17**, 1559–1565 (1997).
3. L. M. McIntosh, M. Jackson, H. H. Mantsch, M. F. Stranc, D. Pilavdzic, and A. N. Crowson, "Infrared spectra of basal cell carcinomas are distinct from non-tumor-bearing components," *J. Invest. Dermatol.* **112**, 951–956 (1999).
4. M. Rajadhyaksha, G. Menaker, T. Flotte, P. Dwyer, and S. Gonzales, "Confocal examination of nonmelanoma cancers in thick skin excisions to potentially guide Mohs micrographic surgery without frozen histopatology," *J. Invest. Dermatol.* **117**, 1137–1143 (2001).
5. A. N. Yaroslavsky, J. Barbosa, V. Neel, C. DiMarzio, and R. R. Anderson, "Combining multispectral polarized light imaging and confocal microscopy for localization of nonmelanoma skin cancer," *J. Biomed. Opt.* **10**(1), 1–6 (2005).
6. S. L. Jacques, J. C. Ramella-Roman, and K. Lee, "Imaging skin pathology with polarized light," *J. Biomed. Opt.* **7**(3), 329–340 (2002).
7. S. L. Jacques, J. C. Ramella-Roman, and K. Lee, "Imaging superficial tissues with polarized light," *Lasers Surg. Med.* **26**(2), 119–129 (2000).
8. W. B. Gill, J. L. Huffman, E. S. Lyon, D. H. Bagley, H. W. Schoenberg, and F. H. Straus II, "Selective surface staining of bladder tumors by intravesical methylene blue with enhanced endoscopic identification," *Cancer* **53**, 2724–2727 (1984).
9. A. M. Wennberg, F. Gudmundson, B. Stenquist, A. Ternesten, L. Molne, A. Rosen, and O. Larko, "In vivo detection of basal cell carcinoma using imaging spectroscopy," *Acta Derm Venereol* **80**(2), 152 (2000).
10. K. G. Gross, H. K. Steinman, and R. P. Rapini, Eds., *Mohs Surgery. Fundamentals and Techniques*, Mosby, St. Louis (1999).
11. A. N. Yaroslavsky, V. Neel, and R. R. Anderson, "Demarcation of nonmelanoma skin cancer margins in thick excisions using multispectral polarized light imaging," *J. Invest. Dermatol.* **121**, 259–266 (2003).

12. A. N. Yaroslavsky, V. Neel, and R. R. Anderson, "Fluorescence polarization imaging for delineating nonmelanoma skin cancers," *Opt. Lett.* **29**(17), 2010–2012 (2004).
13. R. R. Anderson and J. A. Parrish, "Skin optics," *J. Invest. Dermatol.* **77**, 13–19 (1981).
14. S. L. Jacques, C. A. Alter, and S. A. Prahl, "Angular dependence of He-Ne laser light scattering by human dermis," *Lasers Life Sci.* **1**, 309–334 (1987).
15. S. Prahl, "Light transport in tissue," PhD diss., University of Texas at Austin (1988).
16. C. R. Simpson, M. Kohl, M. Essenpreis, and M. Cope, "Near infrared optical properties of *ex vivo* human skin and subcutaneous tissues measured using Monte Carlo inversion technique," *Phys. Med. Biol.* **43**, 2465–2478 (1998).
17. T. Throy and S. N. Thennadil, "Optical properties of human skin in the near infrared wavelength range of 1000 to 2200 nm," *J. Biomed. Opt.* **6**(2), 167–176 (2001).
18. J. D. Hardy, H. T. Hammel, and Dorothy Murgatroyd, "Spectral transmittance and reflectance of excised human skin," *J. Appl. Physiol.* **9**, 257–264 (1956).
19. S. Wan, R. R. Anderson, and J. A. Parrish, "Analytical modeling for the optical properties of the skin with in vitro and in vivo applications," *Photochem. Photobiol.* **34**, 493–499 (1981).
20. J. W. Pickering, S. A. Prahl, N. van Wieringen, J. F. Beek, H. J. C. M. Sterenborg, and M. J. C. van Gemert, "Double-integrating sphere system for measuring the optical properties of tissue," *Appl. Opt.* **32**, 399–410 (1993).
21. I. V. Yaroslavsky, A. N. Yaroslavsky, T. Goldbach, and H.-J. Schwarzmaier, "Inverse hybrid technique for determining the optical properties of turbid media from integrating-sphere measurements," *Appl. Opt.* **35**, 6797–6809 (1996).
22. J. E. Dennis and R. B. Schnabel, *Numerical Methods for Unconstrained Optimization and Nonlinear Equations*, Prentice-Hall, Englewood Cliffs, NJ (1983).
23. A. N. Yaroslavsky, T. Goldbach, I. V. Yaroslavsky, and H.-J. Schwarzmaier, "Different phase-function approximations to determine optical properties of blood: A comparison," *Proc. SPIE* **2982**, 324–330 (1997).
24. G. Müller and A. Roggan, Eds., *Laser-Induced Interstitial Thermotherapy*, SPIE Press, Bellingham, WA (1995).
25. F. A. Duck, *Physical Properties of Tissues. A Comprehensive Reference Book*, Academic Press, London (1990).
26. F. P. Bolin, L. E. Preuss, R. C. Taylor, and R. J. Ference, "Refractive index of some mammalian tissues," *Appl. Opt.* **28**, 2297–2303 (1989).
27. A. N. Yaroslavsky, P. C. Schulze, I. V. Yaroslavsky, R. Shober, F. Ulrich, and H.-J. Schwarzmaier, "Optical properties of selected native and coagulated human brain tissues in vitro in the visible and near infrared spectral range," *Phys. Med. Biol.* **47**, 2059–2073 (2002).
28. D. J. Maitland, J. T. Walsh, Jr., and J. B. Prystowsky, "Optical properties of human gallbladder tissue and bile," *Appl. Opt.* **32**(4), 586–591 (1993).
29. A. Roggan, M. Friebel, K. Dörschel, A. Hahn, and G. Müller, "Optical properties of circulating human blood in the wavelength range 400–2500 nm," *J. Biomed. Opt.* **4**(1), 36–46 (1999).
30. T. Yamashita, T. Kuwahara, S. Gonzales, and M. Takahashi, "Noninvasive visualization of melanin and melanocytes in reflectance mode confocal microscopy," *J. Invest. Dermatol.* **124**, 235–240 (2005).
31. S. L. Jacques, "Origins of tissue optical properties in the UVA, visible and NIR regions," in *OSA TOPS on Advances in Optical Imaging and Photon Migration 2*, R. R. Alfano and J. G. Fujimoto, Eds., pp. 364–371, Optical Society of America, Washington, DC (1996).
32. L. M. McIntosh, R. Summers, M. Jackson, H. H. Mantsch, J. R. Mansfield, M. Howlett, A. N. Crowson, and J. W. Toole, "Towards non-invasive screening of skin lesions by near-infrared spectroscopy," *J. Invest. Dermatol.* **116**, 175–181 (2001).